Calycosin attenuates mitochondrial damage and pyroptosis in heart failure via the Nrf2/ROS/TXNIP pathway

HUA-JING YUAN[1], QUAN-CHENG HAN[1], YI-DING YU[1], HUI YU[1], XIU-JUAN LIU[2], YI-TAO XUE[2] and YAN LI[2]

[1]The First Clinical Medical College, Shandong University of Traditional Chinese Medicine, Jinan, Shandong 250014, P.R. China; [2]Department of Cardiology, Affiliated Hospital of Shandong University of Traditional Chinese Medicine, Jinan, Shandong 250014, P.R. China

Received June 30, 2025; Accepted September 3, 2025

DOI: 10.3892/ijmm.2025.5653

Abstract. Heart failure (HF) is a key public health concern worldwide due to its high morbidity and mortality rates. Calycosin (CA) is a flavonoid natural product that effectively treats HF with cardioprotective effects; however, its mechanism of action remains unclear. The present study aimed to investigate the therapeutic effect of CA on HF and its mechanism through *in vivo* and *in vitro* experiments, and to reveal the roles of pyroptosis and mitochondrial dysfunction in the pathophysiology of HF. The HF model was constructed 4 weeks after ligation of the left anterior descending artery in rats. Myocardial ischemia-reperfusion injury was simulated using a hypoxia-reoxygenation model and nuclear factor erythroid 2-related factor (Nrf2) was silenced by transfection using small interfering RNA to further explore the therapeutic mechanism of CA. The results revealed that CA treatment improved cardiac function and myocardial injury, suppressed oxidative stress levels and improved mitochondrial ultrastructure in HF-induced rats. CA downregulated the expression of relevant pyroptosis proteins via the Nrf2/reactive oxygen species (ROS)/thioredoxin-interacting protein (TXNIP) pathway. *In vitro* experiments demonstrated consistent results confirming that CA ameliorated mitochondrial damage by reducing levels of ROS and inhibiting mitochondrial gasdermin D N-terminal fragments activation. Silencing Nrf2 partially reversed the cardioprotective effects of CA, confirming the key therapeutic role of CA in Nrf2-mediated anti-pyroptosis. In conclusion, CA inhibits pyroptosis and improves mitochondrial damage in HF through the Nrf2/ROS/TXNIP pathway, which may disrupt the crosstalk between mitochondrial damage and pyroptosis, thereby exerting cardioprotective effects.

Correspondence to: Dr Yi-Tao Xue or Dr Yan Li, Department of Cardiology, Affiliated Hospital of Shandong University of Traditional Chinese Medicine, 16369 Jingshi Road, Jinan, Shandong 250014, P.R. China
E-mail: xytsdzydfy@126.com
E-mail: liyan88130@163.com

Abbreviations: ASC, apoptosis-associated speck-like protein containing a CARD; CA, calycosin; CA-L, CA low-dose; CA-H, CA high-dose; CAP, captopril; CCK-8, Cell Counting Kit-8; ECAR, extracellular acidification rate; FCCP, Trifluoromethoxy carbonylcyanide phenylhydrazone, Carbonyl cyanide 4-(trifluoromethoxy)phenylhydrazone; FS, fractional shortening; GSDMD, gasdermin D; GSDMD-NT, GSDMD N-terminal fragments; HF, heart failure; H/R, hypoxia-reoxygenation; Keap1, Kelch-like ECH-associated protein 1; LAD, left anterior descending; LDH, lactate dehydrogenase; LVEF, left ventricular ejection fraction; MDA, malondialdehyde; NLRP3, NLR family pyrin domain-containing protein 3; Nrf2, nuclear factor erythroid 2-related factor; NT-proBNP, N-terminal pro B-type natriuretic peptide; OCR, oxygen consumption rate; ROS, reactive oxygen species; SOD, superoxide dismutase; TEM, transmission electron microscopy; T-GSH/GSSG, total glutathione/glutathione disulfide; TRX, thioredoxin; TXNIP, thioredoxin-interacting protein

Key words: CA, mitochondrial damage, pyroptosis, HF, Nrf2, ROS, TXNIP

Introduction

Heart failure (HF), one of the end-stage manifestations of cardiovascular disease has an estimated prevalence of ≥56 million individuals and a 5-year survival rate following diagnosis remaining >50%. Consequently, it has been recognized as an important issue in public health and a major cause of morbidity and mortality worldwide (1,2). HF not only considerably affects the quality of life of patients, but may also lead to serious complications and can be life-threatening (3). Despite improvements in the guidelines for the treatment of HF, and the development of new drugs and clinical studies, such as intravenous recombinant human Neuregulin-1 and vericiguat (4,5), the management of this condition remains challenging, especially in terms of prognosis (6).

Previous studies have revealed that oxidative stress, mitochondrial dysfunction, calcium regulation and cell death are associated with the onset and progression of HF (7-10). Notably, pyroptosis, a mode of programmed cell death, has been shown to be associated with HF (11). Pyroptosis is mainly mediated by gasdermin D (GSDMD), which causes cell membrane rupture through the generation of GSDMD N-terminal fragments (GSDMD-NT) with pore-forming activity, resulting in the release of inflammatory factors, and exacerbating cell death and tissue damage (12). A recent study revealed that GSDMD-NT perforates the mitochondrial

membrane in pyroptosis, leading to mitochondrial damage and inducing reactive oxygen species (ROS) release. ROS further amplifies GSDMD binding and mitochondrial damage in pyroptosis (13). Excessive release of ROS can activate the NLR family pyrin domain-containing protein 3 (NLRP3) inflammasome in a positive cascade reaction with thioredoxin-interacting protein (TXNIP), thereby mediating the occurrence of pyroptosis (14). Nuclear factor erythroid 2-related factor (Nrf2) is a key regulator of the antioxidant response and can regulate oxidative stress by eliminating ROS and inhibiting TXNIP expression (15,16).

Calycosin (CA) is a natural flavonoid compound that has been demonstrated to exert various biological effects, including anti-inflammatory, antioxidant and pro-angiogenic properties (17). CA has a broad application prospect in the treatment of cardiovascular diseases, and studies have revealed that CA can improve myocardial oxidative stress (18), attenuate myocardial fibrosis and cardiac dysfunction after myocardial infarction, and inhibit HF after acute infarction (19,20). Previous studies have revealed that CA inhibits pyroptosis and ameliorates myocardial injury by inhibiting the activation of the NLRP3 inflammasome (21,22). In addition, CA may upregulate Nrf2 expression, and ameliorate myocardial oxidative stress and mitochondrial damage, thereby protecting the myocardium (23). Therefore, the present study further explored the therapeutic mechanism of CA based on the Nrf2/ROS/TXNIP pathway-mediated mitochondrial damage and pyroptosis in HF.

Materials and methods

Reagents. CA was purchased from Shanghai Yuanye Biotechnology Co., Ltd. Captopril (CAP; CAP purchase specification: 25 mg; national drug approval number: H44021595) was used as the positive control and was purchased from Guangdong Pidi Pharmaceutical Co., Ltd. Detection kit information was as follows: Rat N-terminal pro B-type natriuretic peptide (NT-proBNP) ELISA Kit (cat. no. CSB-E08752r) was purchased from Cusabio Technology, LLC; lactate dehydrogenase (LDH) ELISA kit (cat. no. SEB864Ra) was purchased from CLOUD-CLONE CORP, CCC; malondialdehyde (MDA) assay kit (cat. no. A003-1), superoxide dismutase (SOD) assay kit (cat. no. A001-3-2) and microplate method total glutathione/glutathione disulfide (T-GSH/GSSG) assay kit (cat. no. A061-1-1) were purchased from Nanjing Jiancheng Bioengineering Institute. LDH cytotoxicity colorimetric assay kit (cat. no. E-BC-K771-M) was purchased from Elabscience. Antibody information was as follows: Nrf2 (cat. no. 80593-1-RR), apoptosis-associated speck-like protein containing a CARD (ASC; cat. no. 67494-1-Ig), IL-1β (cat. no. 29530-1-AP), cytochrome *c* (cat. no. 66264-1-Ig) and β-actin (cat. no. 66009-1-Ig) antibodies were purchased from Proteintech Group, Inc.; TXNIP (cat. no. A9342), NLRP3 (cat. no. A5652), IL-18 (cat. no. A23076) and GSDMD (full length and N terminal; cat. no. A24476) antibodies were purchased from ABclonal Biotech Co., Ltd.; Caspase-1 (pro- and cleaved-Caspase-1) (cat. no. ab286125), COX IV (cat. no. ab16056), Goat Anti-rabbit IgG HRP (cat. no. ab150077) and Goat Anti-Mouse IgG HRP (cat. no. ab205719) antibodies were purchased from Abcam. Mitochondrial membrane potential assay kit JC-1 (cat. no. C2006), ROS Assay kit (cat. no. S0033S) and MitoSOX Red assay kit (cat. no. S0061S) were purchased from Beyotime Institute of Biotechnology. Masson Tricolor Staining kit (cat. no. G1006) was purchased from Wuhan Servicebio Technology Co., Ltd. Cell mitochondrial stress test kit (cat. no. 103015-100), glycolytic stress test kit (cat. no. 103020-100) and Seahorse XF base medium (cat. no. 102353-100) were purchased from Agilent Technologies, Inc.

Establishment and treatment of rats. A total of 50 8-week-old male Wistar rats (weight, 180-220 g) were purchased from Beijing Vital River Laboratory Animal Technology Co., Ltd. The rats were housed in the Experimental Center of the Affiliated Hospital of Shandong University of Traditional Chinese Medicine (Jinan, China) under standard conditions (12-h light/dark cycle with free access to water and food). The animal experimental procedures were approved by the Experimental Animal Management Committee and the Ethics Committee of the Affiliated Hospital of Shandong University of Traditional Chinese Medicine. The animal experiments strictly followed the guidelines of the Ethics Committee.

Rats were randomly divided into five groups: Sham, HF, CA low-dose (CA-L), CA high-dose (CA-H) and CAP group (n=10/group). In the present study, the HF model was constructed 4 weeks after ligation of the left anterior descending (LAD) artery in rats. Specifically, rats were anesthetized using 2-3% isoflurane (3% induction and 2% maintenance) based on an isoflurane delivery system. The left chest area of the rats was fully exposed under aseptic conditions. The left chest area of the rats was shaved and disinfected to ensure aseptic conditions. A minimally invasive open thoracotomy was performed in the fourth intercostal space and the LAD artery was permanently ligated using a 6-0 suture. After ligation and squeezing out the gas from the chest cavity, the muscle and skin were sutured at the surgical site layer by layer. The Sham group underwent the same surgical procedures, but the sutures were only passed through the LAD artery without ligation. After 4 weeks, echocardiography was used to determine whether the HF rat model was successfully constructed. CA was dissolved in DMSO to prepare a 60 mg/ml stock solution, which was then diluted to the appropriate working concentration using saline containing 20% Sulfobutylether-β-Cyclodextrin (SBE-β-CD, Proteintech Group, Inc.) according to experimental requirements. Subsequently, CA-L and CA-H rats received intraperitoneal injections of 15 and 30 mg/kg CA, respectively, daily for 4 weeks (24). The CAP group rats received 10 mg/kg CAP administered orally by gavage daily for 4 weeks. The Sham and HF groups received intraperitoneal injections of 5 ml/kg saline containing 20% SBE-β-CD daily for 4 weeks. Following echocardiography and cardiac puncture for blood sampling, the rats were euthanized through CO_2 asphyxia (40% vol/min) for 5 min and death was confirmed by the absence of respiration and heartbeat. Following euthanasia, rat hearts were immediately collected. Due to limited tissue available from each rat, the sample sizes used in each experiment varied. The following criteria were established as humane endpoints: i) Weight loss >20% of the initial body weight; ii) prolonged feeding impairment or mobility deficits; iii) rats exhibited signs of depression accompanied by hypothermia when not under anesthesia.

Echocardiography. At 4 weeks after surgery and treatment, echocardiography was carried out on all rats to assess cardiac function, in order to verify the construction of the HF model and the therapeutic effect of CA. Specifically, after anesthetizing rats with 2-3% isoflurane (3% induction and 2% maintenance) based on an isoflurane delivery system, 2D long-axis images were recorded using a portable Mindray M5 digital ultrasound scanner (Shenzhen Mindray Bio-Medical Electronics Co., Ltd.). During three cardiac cycles, left ventricular ejection fraction (LVEF) and fractional shortening (FS) were measured at the myocardial level using the M-mode.

Histological analyses. A total of three fresh rat myocardial tissue samples in each group were fixed in 4% paraformaldehyde (cat. no. G1101-500ML, Wuhan Servicebio Technology Co., Ltd.) at room temperature for 24 h according to the instructions of the manufacturer that supplied the paraformaldehyde, embedded in paraffin and cut into 4-μm sections. Sections were stained at room temperature with hematoxylin solution for 5 min, followed by 15 sec in eosin solution for H&E staining. Sections were stained at room temperature with Masson dye solution set at room temperature according to the manufacturer's instructions for Masson's trichrome staining. Images were obtained and histopathological status was assessed using a digital section scanner (WS-10; Zhiyue Medical Technology (Jiangsu) Co., Ltd.). Masson's trichrome staining results were analyzed using ImageJ 1.52v software (National Institutes of Health).

Transmission electron microscopy (TEM). Three left ventricular myocardial tissue samples in each group were rinsed three times in pre-cooled PBS buffer, cut into 1-2 mm^3 pieces and fixed in 2.5% glutaraldehyde at 4˚C for 24 h. The myocardial tissues were subsequently dehydrated in a graded ethanol series, transitioned with propylene oxide and embedded in Epon812 epoxy resin at 60˚C for 48 h. Ultrathin sections (70 nm) were cut using an ultramicrotome, collected on 200-mesh copper grids and dual-stained with 2% uranyl acetate and lead citrate, both at room temperature for 15 min. Sections were examined by TEM, focusing on mitochondrial morphology, cristae integrity and myofibril arrangement.

Measurement of NT-proBNP, T-GSH/GSSG, MDA, SOD and LDH. After anesthetizing the rats with isoflurane to carry out echocardiography, 1 ml blood was collected through cardiac puncture. Rat serum was isolated from blood by centrifuging at 1,500 x g for 10 min at 4˚C. NT-proBNP and LDH levels in the serum samples were assessed at an absorbance of 450 nm according to the standard procedure of the assay kits. Following cardiac puncture for blood sampling, all rats were euthanized, and their hearts were immediately collected. After isolation of five rat myocardial tissue samples, the levels of T-GSH/GSSG, SOD and MDA in myocardial tissues were detected using the assay kits, according to the standard procedures of the test kits. Absorbance was measured at 405, 450 and 532 nm using a microplate reader to detect T-GSH/GSSG, SOD and MDA levels, respectively. Post-treatment, LDH levels in cells were assessed at an absorbance of 450 nm according to the standard procedure of the assay kits.

Immunohistochemistry staining. The paraffin-embedded myocardial tissue sections were subjected for thermally repaired antigen using citrate buffer (pH 6.0) at 95-100˚C. Following natural cooling, they were washed three times with PBS. Hydrogen peroxide (3%) solution was used to inactivate endogenous enzymes. Subsequently, the sections were incubated with Nrf2 antibody (1:500) at 4˚C overnight, then sections were incubated with the Goat Anti-rabbit IgG HRP secondary antibody (1:1,000) for 1 h at room temperature. The sections were immersed in diaminobenzidine, counterstained with hematoxylin and finally imaged using a digital section scanner (WS-10; Zhiyue Medical Technology (Jiangsu) Co., Ltd.). The results were analyzed using ImageJ 1.52v software (National Institutes of Health).

Cell culture and treatments. Rat H9c2 cardiomyocytes were purchased from The Cell Bank of Type Culture Collection of The Chinese Academy of Sciences and cultured in DMEM (Pricella Biotechnology) supplemented with 10% fetal bovine serum (Vazyme Biotech Co., Ltd.) and 1% penicillin/streptomycin at 37˚C with 5% CO_2. The present study employed a hypoxia-reoxygenation (H/R) model to simulate myocardial ischemia-reperfusion injury. CA was dissolved in DMSO to prepare a 0.1 M stock solution, which was then diluted to the appropriate working concentration according to experimental requirements. After model establishment, the experimental groups were treated with CA solutions at different concentrations (10, 20 and 30 μM). Meanwhile, control and model groups were established and treated with an equivalent concentration of DMSO (0.03%) solution to eliminate solvent interference.

The method used to establish the H/R model for cardiomyocytes was as follows: First, cultured cardiomyocytes were placed in a hypoxia chamber with gas conditions adjusted to 1% O_2, 5% CO_2 and 94% N_2, and incubated at 37˚C for 12 h to simulate a hypoxic environment. After the hypoxia period, the cells were transferred to a normoxic incubator with gas conditions of 20% O_2, 5% CO_2 and 75% N_2, and incubated at 37˚C for 24 h to simulate the reoxygenation process. Throughout the experiment, the temperature, humidity and gas concentration within the incubator were strictly controlled, and cell status was regularly monitored to ensure the reproducibility and stability of the model (25).

Cell transfection [small interfering RNA (siRNA)-Nrf2]. Cell transfection was performed before H/R and/or CA treatment. Pooled siRNAs targeting Nrf2 (#1, #2 and #3) were used to effectively silence Nrf2 and eliminate off-target effects. The siRNA sequences were as follows: Nrf2#1, forward 5'-GGAAGUCUUCAGCAUGUUATT-3' and reverse 5'-UAACAUGCUGAAGACUUCCTT-3'; Nrf2#2, forward 5'-CGAGAAGUGUUUGACUUUATT-3' and reverse 5'-UAAAGUCAAACACUUCUCGTT-3'; Nrf2#3, forward 5'-GGGUUCAGUGACUCGGAAATT-3' and reverse 5'-UUUCCGAGUCACUGAACCCTT-3'; non-targeting negative control (NC), forward 5'-UUCUCCGAACGUGUCACG UTT -3' and reverse 5'-ACGUGACACGUUCGGAGAATT-3' (Beijing Tsingke Biotech Co., Ltd.). H9c2 cells were seeded in 6-well plates at 1x10^5 cells/well and were treated at 37˚C with 5% CO_2 until they reached 70-80% confluence. The 6-well plate for transfection was prepared by discarding the

medium, washing with PBS and adding 1.5 ml Opti-MEM (Invitrogen; Thermo Fisher Scientific, Inc.) per well. For each experimental group, 1.5-ml Eppendorf tubes were labeled and 250 μl Opti-MEM with 5 μl Lipofectamine™ 3000 (Invitrogen; Thermo Fisher Scientific, Inc.) was added, mixed by pipetting and incubated at room temperature for 5 min. Similarly, labeled tubes were prepared with 250 μl Opti-MEM and 8 μl siRNA (concentration, 20 μM), mixed by pipetting. The siRNA mixture was combined with the corresponding Lipofectamine 3000 mixture, mixed thoroughly and incubated at room temperature for 20 min. The mixture was then added to the 6-well plate and the medium was replaced after 8 h at room temperature. Cell functional assays were conducted 48 h later.

Cell Counting Kit-8 (CCK-8) assay. A H9c2 cell suspension was seeded in a 96-well plate at 100 μl/well and incubated at 37˚C with 5% CO_2 for 24 h to allow cell attachment and proliferation. Different concentrations of CA (0, 5, 10, 20, 30, 40 and 50 μM) were added to each well, followed by an additional 24-h incubation. For evaluating the protective effect of CA on H/R-induced cardiomyocyte injury, cells were subjected to CA treatment following H/R treatment; otherwise, this step was omitted for assessing the direct impact of CA on cell viability. After incubation, 10 μl CCK-8 solution (Vazyme Biotech Co, Ltd.) was added to each well, gently mixed and incubated for 2 h. The absorbance (OD value) of each well was measured at 450 nm using a microplate reader and cell viability was calculated to evaluate the effects of different CA concentrations on H9c2 cell viability.

ROS detection. To evaluate intracellular ROS levels, a commercially available ROS assay kit (cat. no. S0033S; Beyotime Institute of Biotechnology) was employed. H9c2 cells were seeded in a 6-well plate and cultured until they reached 70-80% confluence. Post-treatment, the cell suspension was collected and transferred to centrifuge tubes, followed by centrifugation at 200 x g at room temperature for 5 min to pellet the cells, after which the supernatant was carefully removed. The fluorescent probe 2',7'-dichlorodihydrofluorescein diacetate (DCFH-DA) was diluted at a ratio of 1:1,000 in serum-free medium to achieve a final concentration of 10 μM and 1 ml of the diluted solution was added to each tube. The cells were then incubated at 37˚C for 20 min to facilitate the uptake of DCFH-DA. After incubation, the cells were washed twice with serum-free medium, with centrifugation at 200 x g at room temperature for 5 min after each wash. Finally, the cell pellets were resuspended in 200 μl serum-free culture medium and ROS levels were quantified using flow cytometry (C6 Plus; Becton, Dickinson and Company) and observed under a fluorescence microscope. The data were analyzed using FlowJo 10.6.2 (BD Biosciences).

Mitochondrial ROS staining. H9c2 cells inoculated in 6-well plates were collected. Detection of mitochondrial ROS levels was performed using the MitoSOX Red assay kit according to the manufacturer's instructions. Cells were washed with PBS and were then examined under a fluorescence microscope.

Immunofluorescence staining. H9c2 cells were seeded on coverslips in 24-well plates and grown to 70% confluence before treatment. Post-treatment, the plates were washed twice with PBS. Fixation was carried out with 200 μl immunol staining fix solution (Beyotime Institute of Biotechnology) per well for 20 min at room temperature, followed by two washes with PBS. Permeabilization was carried out with 200 μl immunostaining permeabilization buffer with Triton X-100 (Beyotime Institute of Biotechnology) for 10 min at room temperature, and the cells were washed twice with PBS. Blocking was achieved with 200 μl 5% BSA for 1 h at room temperature, followed by two washes with PBS. A Nrf2 primary antibody (1:500) was then added (200 μl/well) and incubated overnight at 4˚C, followed by two washes with PBS. Subsequently, a secondary antibody Goat Anti-rabbit IgG HRP (1:500) was added (200 μl/well) and incubated overnight at 4˚C or for 90 min at room temperature, followed by two washes with PBS. DAPI staining was carried out (200 μl/well) for 10 min at room temperature and the samples were then washed twice with PBS. Finally, cells were mounted with antifade medium and images were captured under a fluorescence microscope.

Annexin V-FITC/PI staining. Annexin V-FITC/PI detection kit (Vazyme Biotech Co, Ltd.) was used to detect cell death. H9c2 cells were seeded in 6-well plates at $1x10^5$ cells/well and were cultured at 37˚C with 5% CO_2 until they reached 70-80% confluence. Post-treatment, the cells were collected and adherent cells were digested using EDTA-free trypsin for 2 min. Cells were then stained with 5 μl Annexin V-FITC and 5 μl PI staining solution, incubated in the dark at room temperature for 10 min and mixed with 400 μl 1x Binding Buffer. Stained cells were analyzed by flow cytometry (C6 Plus, Becton, Dickinson and Company) within 1 h and the data were analyzed using FlowJo 10.6.2 (BD Biosciences).

Mitochondrial membrane potential assay with JC-1. Cells were seeded in 6-well plates and cultured until treatment was completed. The JC-1 working solution was prepared according to the standard procedure of the JC-1 staining kit. Cells were incubated with JC-1 working solution at 37˚C for 20 min and analyzed using flow cytometry.

Cellular energy metabolism analysis. H9c2 cells were seeded in 6-well plates at $1x10^5$ cells/well and were cultured at 37˚C with 5% CO_2 until they reached 70-80% confluence. Detection of oxygen consumption rate (OCR) and extracellular acidification rate (ECAR) was performed using the cell mitochondrial stress test kit and glycolytic stress test kit, following the manufacturer's instructions. Post-treatment, cells were incubated with Seahorse XF Base medium at 37˚C, followed by the sequential addition of oligomycin, FCCP [trifluoromethoxy carbonylcyanide phenylhydrazone, Carbonyl cyanide 4-(trifluoromethoxy) phenylhydrazone], rotenone and antimycin A. The Seahorse analyzer [XF96; Agilent Technologies (China) Co., Ltd.] was used to measure OCR and ECAR of the cells.

Western blotting. Three rat myocardial tissue samples in each group were used for Western blotting. Proteins were extracted from cardiac tissues and cells using RIPA buffer (Wuhan Servicebio Technology Co., Ltd.) and PMSF (Beyotime Institute

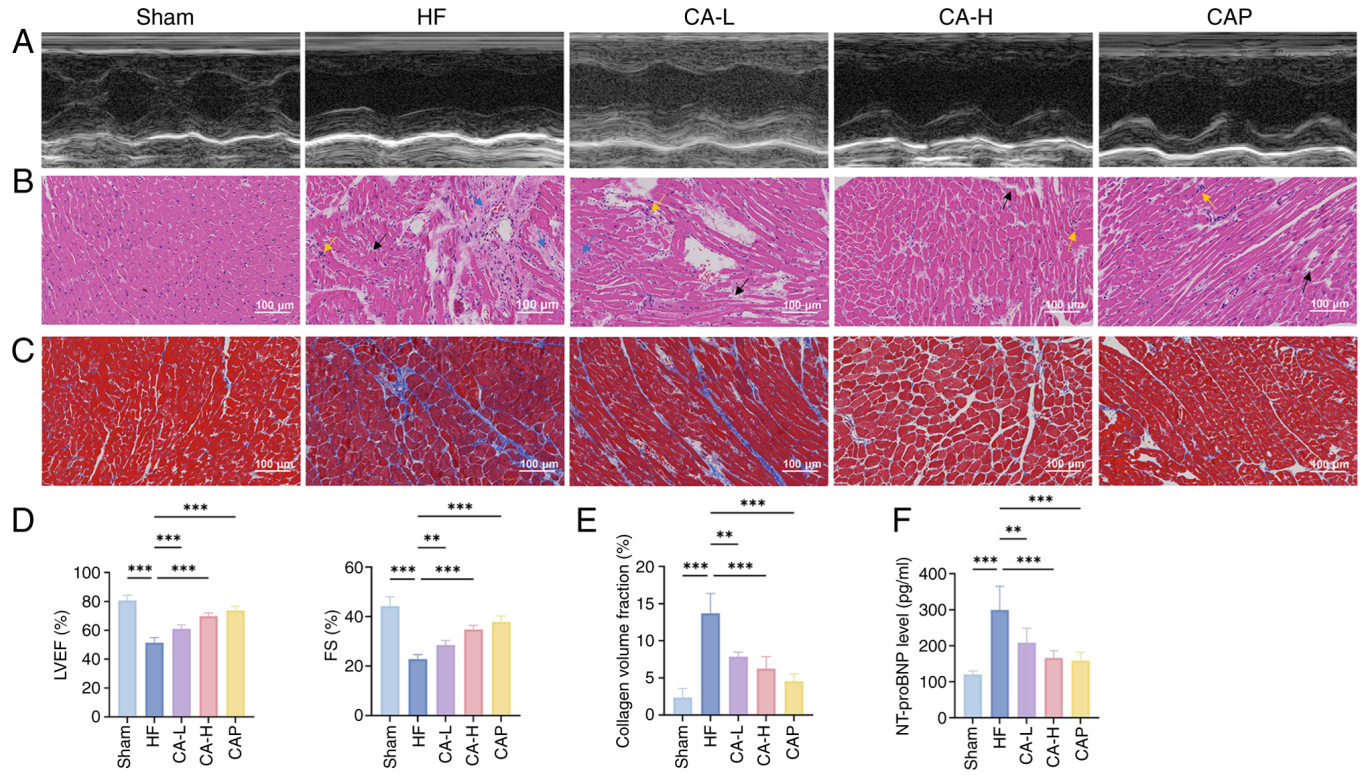

Figure 1. CA effectively improves cardiac function in HF. (A) Representative echocardiography, (B) H&E staining and (C) Masson's trichrome staining images of each group. In H&E staining, the yellow arrows indicate inflammatory infiltration, the black arrows indicate loss of myocardial cells and the blue arrows indicate interstitial fibrosis. (D) Statistical analysis of LVEF and FS of rats in each group, as determined by echocardiography (n=5). (E) Quantitative analysis of Masson's trichrome staining (n=3). (F) Serum NT-proBNP levels in rats of each group (n=5). Data are presented as the mean ± SD, **P<0.01, ***P<0.001. CA, calycosin; HF, heart failure; LVEF, left ventricular ejection fraction; FS, fractional shortening; NT-proBNP, N-terminal pro B-type natriuretic peptide; CA-L, calycosin low-dose; CA-H, calycosin high-dose; CAP, captopril.

of Biotechnology). The extraction of mitochondrial proteins from cells was carried out using the mitochondrial isolation and protein extraction kit (Proteintech Group, Inc.). Protein concentrations were quantified using a BCA protein assay kit and samples were adjusted with loading buffer to ensure equal protein loading. A total of 20 μg protein was then separated by SDS-PAGE on 10% gels and transferred onto a PVDF membrane. To minimize non-specific binding, the membrane was blocked with 5% skim milk at room temperature for 1 h. Subsequently, the membrane was incubated at the appropriate dilutions overnight at 4˚C with the primary antibodies: Nrf2 (1:1,000), TXNIP (1:1,000), NLRP3 (1:1,000), ASC (1:5,000), Caspase-1 (1:500), GSDMD (1:1,000), IL-1β (1:1,000), IL-18 (1:1,000), COX IV (1:2,000) and β-actin (1:50,000). Unbound primary antibodies were removed by washing the membrane with PBS. The membrane was then incubated with Goat Anti-rabbit IgG HRP and Goat Anti-Mouse IgG HRP secondary antibodies (1:10,000) at room temperature for 1 h to facilitate antibody-antigen complex formation. Excess secondary antibody was removed by additional PBS washes. For detection, the membrane was incubated with electrochemiluminescence substrate solution (Vazyme Biotech Co, Ltd.) for 3 min in the dark before imaging. β-actin and COX IV were used as loading controls for total protein and mitochondrial protein expression, respectively. Band intensities were semi-quantified using ImageJ 1.52v software (National Institutes of Health), with β-actin/COX IV serving as the internal control for normalization. The relative expression levels of the target proteins were calculated as the ratio of the target protein band density to the β-actin/COX IV band density.

Statistical analysis. Data analysis was performed using SPSS Statistics 27.0 (IBM Corp.) and GraphPad Prism 10 software (Dotmatics). All *in vitro* experimental data are presented from three independent experiments. Continuous variables were presented as mean ± SD. Group comparisons were conducted using one-way analysis of variance followed by Dunnett's post hoc test. Two-way analysis of variance and post hoc tests were used to compare two variables (siRNA and treatment). P<0.05 was considered to indicate a statistically significant difference.

Results

CA effectively improves cardiac function and mitochondrial damage in HF-induced rats. Echocardiography was used to assess cardiac function in rats (Fig. 1A) and the results revealed that LVEF and FS were significantly reduced in the HF group compared with those in the Sham group. By contrast, treatment with both doses of CA and with CAP exhibited improved LVEF and FS (Fig. 1D). H&E and Masson's trichrome staining further revealed that the myocardial tissues of HF rats exhibited notable inflammatory infiltration, cellular loss, disarrangement and interstitial fibrosis, whereas CA and CAP treatment ameliorated the severity of myocardial lesions (Fig. 1B, C and E). In addition, CA and CAP treatment effectively reduced levels of NT-pro BNP in HF-induced rats (Fig. 1F).

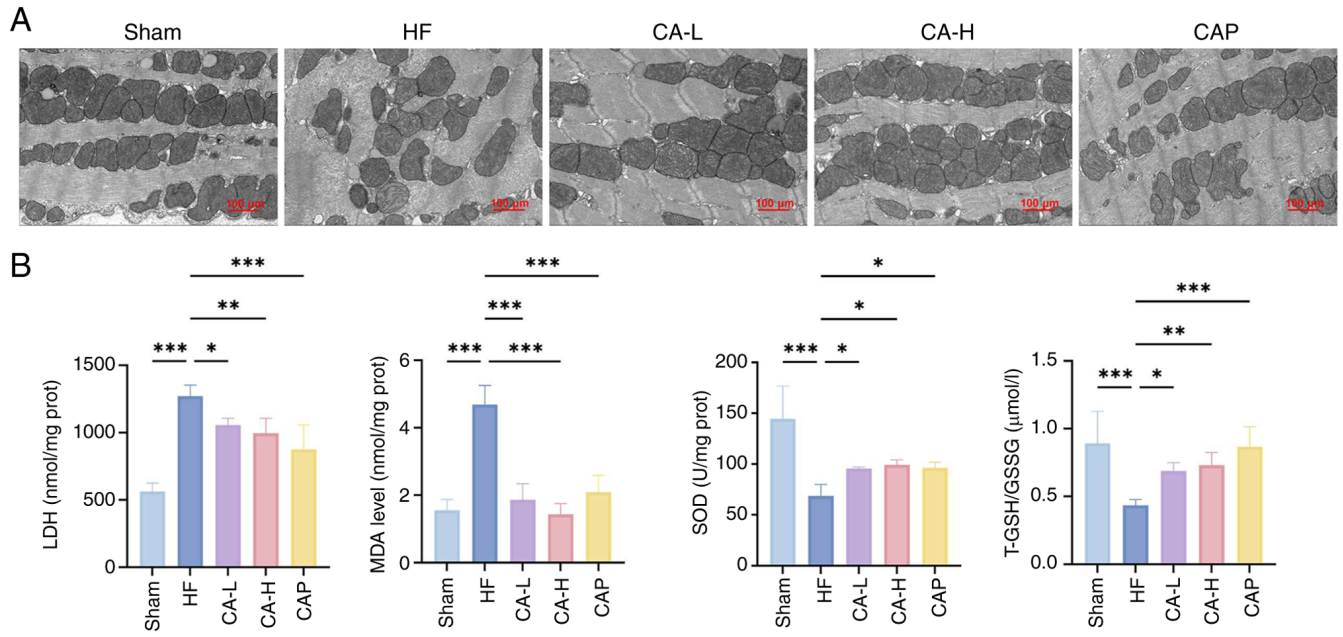

Figure 2. CA effectively improves mitochondrial damage and cardiac oxidative stress in HF. (A) Representative transmission electron microscopy images of rats in each group. (B) Levels of oxidative stress-related indicators (n=5). Data are presented as the mean ± SD, *P<0.05, **P<0.01, ***P<0.001. CA, calycosin; HF, heart failure; CA-L, calycosin low-dose; CA-H, calycosin high-dose; CAP, captopril; LDH, lactate dehydrogenase; MDA, malondialdehyde; SOD, superoxide dismutase; GSH, glutathione; GSSG, GSH disulfide.

TEM was used to observe mitochondrial morphology in the HF-induced rat myocardium. In addition, the oxidative stress-related indicators LDH, MDA, SOD and T-GSH/GSSG were measured to assess the levels of oxidative stress in the HF-induced rat myocardium. TEM revealed that in the Sham group, the mitochondria were neatly arranged, the membrane structure was intact and the cristae were densely structured (Fig. 2A). In the HF group, mitochondrial arrangement was disorganized, cristae were broken, mitochondria were swollen and the membrane structure was damaged. By contrast, CA and CAP treatment resulted in an improvement in mitochondrial swelling, cristae breakage and relative membrane structural integrity. In addition, rats with HF exhibited elevated levels of LDH and MDA, and decreased levels of SOD and T-GSH/GSSG, indicating significant oxidative stress in HF, which was significantly prevented by CA and CAP treatment (Fig. 2B).

CA inhibits HF-induced pyroptosis via the Nrf2/ROS/TXNIP pathway. To further explore the mechanism of CA in the treatment of HF, the present study measured the expression of proteins in the Nrf2/ROS/TXNIP pathway and related pyroptosis proteins. Immunohistochemistry staining indicated that Nrf2 expression was upregulated in the HF group compared with the Sham group, and was further increased following CA treatment (Fig. 3A). Western blotting results further confirmed that compared with in the Sham group, Nrf2 and TXNIP expression levels were upregulated in HF-induced rats. CA treatment further upregulated the expression levels of Nrf2 and inhibited the expression of TXNIP (Fig. 3B and C). In HF-induced rats, the expression of related pyroptosis proteins and inflammatory cytokines was upregulated, specifically, the NLRP3 inflammasome was activated, and the expression levels of NLRP3, ASC, pro- and cleaved-caspase-1, GSDMD, GSDMD-NT (Fig. 3D and E), IL-18 and IL-1β (Fig. 3F and G) were elevated. By contrast, CA treatment significantly downregulated the expression of these pyroptosis-related proteins and inflammatory cytokines.

CA protects cardiomyocytes and inhibits pyroptosis via the Nrf2/ROS/TXNIP pathway. To further validate the potential cardioprotective effects and therapeutic mechanisms of CA, further experiments were conducted in H/R-treated H9c2 cells. The CCK-8 assay was used to examine the biosafety of CA in H9c2 cells and the results showed that CA was cytotoxic at concentrations ≥40 μM (Fig. 4A). Subsequently, the H/R model was constructed and the cardioprotective effects of CA were evaluated through the CCK-8 assay and by measuring LDH levels. The results showed that H/R treatment significantly reduced cell viability and promoted LDH release, whereas CA treatment dose-dependently reversed this effect (Fig. 4B).

During pyroptosis, GSDMD-NT can form membrane pores in the plasma membrane and mitochondrial membrane, disrupting membrane integrity and thereby leading to mitochondrial damage and cell death, which was observed in the present study by Annexin V/PI staining, with an increase in Annexin V^{+}/PI^{+} cells detected in response to H/R, while CA treatment ameliorated this increase in Annexin V+/PI+ cells (Fig. 4C). Immunofluorescence staining of cardiomyocytes for Nrf2 revealed that Nrf2 levels were increased by H/R treatment and further increased by CA treatment, and that CA promoted Nrf2 translocation to the nucleus (Fig. 4D). Furthermore, detection of intracellular ROS levels revealed elevated ROS release in response to H/R treatment, whereas CA treatment significantly reduced ROS release (Fig. 4E). Western blotting further indicated that H/R treatment upregulated the expression levels of Nrf2, TXNIP, activated the NLRP3 inflammasome and increased the expression levels of NLRP3, ASC, pro- and cleaved-caspase-1, GSDMD, GSDMD-NT,

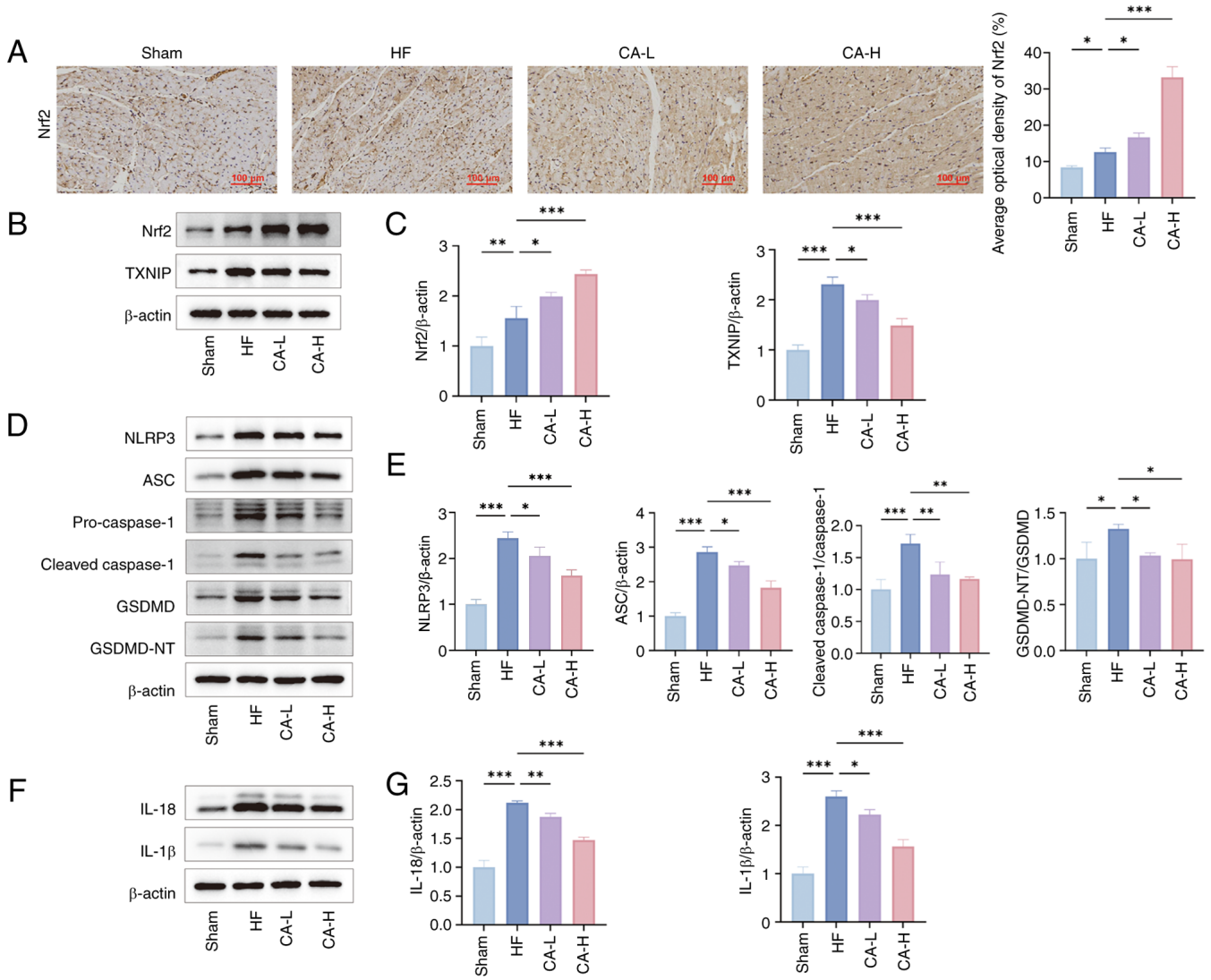

Figure 3. CA improves pyroptosis in HF through the Nrf2/ROS/TXNIP pathway. (A) Representative Nrf2 immunohistochemistry images of each group and their quantitative analysis (n=3). (B) Representative images of the expression levels of Nrf2 and TXNIP in myocardial tissue of Wistar rats assessed by western blotting. (C) Semi-quantitative analysis of Nrf2 and TXNIP expressions (n=3). (D) Representative images of the expression levels of NLRP3, ASC, pro- and cleaved-caspase-1, GSDMD, GSDMD-NT in myocardial tissue of Wistar rats by western blotting. (E) Semi-quantitative analysis of NLRP3, ASC, pro- and cleaved-caspase-1, GSDMD, GSDMD-NT expressions (n=3). (F) Representative images of the expression levels of IL-18 and IL-1β in myocardial tissue of Wistar rats by western blotting. (G) Semi-quantitative analysis of IL-18 and IL-1β expressions (n=3). Data are presented as the mean ± SD, *P<0.05, **P<0.01, ***P<0.001. CA, calycosin; HF, heart failure; Nrf2, nuclear factor erythroid 2-related factor; ROS, reactive oxygen species; TXNIP, thioredoxin-interacting protein; CA-L, calycosin low-dose; CA-H, calycosin high-dose; ASC, apoptosis-associated speck-like protein containing a CARD; GSDMD, gasdermin D; GSDMD-NT, GSDMD N-terminal fragments.

IL-18 and IL-1β. CA treatment further upregulated, the expression of Nrf2, inhibited the expression of TXNIP (Fig. 5A) and suppressed the expression and release of NLRP3, ASC, pro- and cleaved-caspase-1, GSDMD, GSDMD-NT (Fig. 5C), IL-18 and IL-1β (Fig. 5B).

CA improves mitochondrial damage in cardiomyocytes. Since CA protects cardiomyocytes in a dose-dependent manner, CA 30 μM was used in the present study to further investigate the improvement effect on mitochondrial damage. Flow cytometry revealed that H/R treatment significantly decreased mitochondrial membrane potential, while CA treatment prevented this change (Fig. 6A). Furthermore, ROS and mitochondrial ROS staining of the cells revealed an increase in intracellular and mitochondrial ROS with H/R treatment, which was improved by CA treatment (Fig. 6B and C). The ECAR and OCR were used to assess mitochondrial glucose metabolism and oxidative phosphorylation levels. As shown in Fig. 6D, H/R treatment promoted glycolysis and inhibited mitochondrial respiration, while CA treatment ameliorated this mitochondrial damage. In addition, western blotting results indicated that H/R treatment upregulated GSDMD expression levels, promoted GSDMD-NT activation and upregulated cytochrome *c* expression levels in the mitochondria; by contrast, CA treatment downregulated their expression and activation (Fig. 6E).

Silencing Nrf2 inhibits the therapeutic effects of CA. To further validate the therapeutic mechanism of CA, Nrf2 expression was knocked down using siRNA in H9c2 cells. After verifying the efficiency of Nrf2 silencing (Fig. 7A),

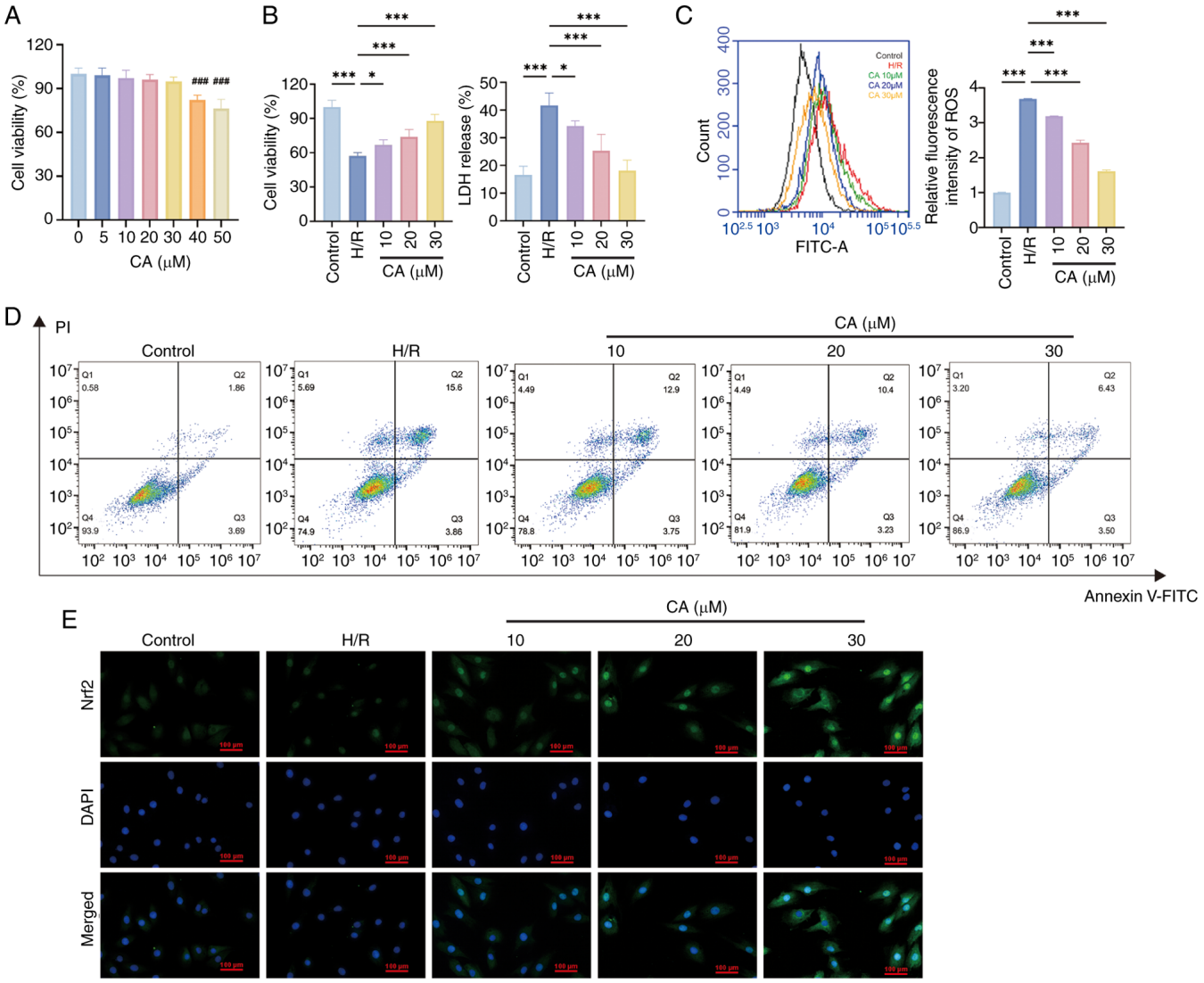

Figure 4. CA protects cardiomyocytes and inhibits pyroptosis. (A) Detection of CA cytotoxicity using a Cell Counting Kit-8 assay (n=3). ###P<0.001, compared with 0, 5, 10, 20, 30 μM groups. (B) Cardiomyocyte protective effects of CA (n=3). (C) Flow cytometric analysis of cell death with Annexin V-FITC/PI staining. (D) Immunofluorescence staining of cardiomyocytes for Nrf2. (E) Detection of intracellular ROS levels in cardiomyocytes (n=3). Data are presented as the mean ± SD, *P<0.05, ***P<0.001. CA, calycosin; Nrf2, nuclear factor erythroid 2-related factor; ROS, reactive oxygen species; H/R, hypoxia-reperfusion; LDH, lactate dehydrogenase.

detection of intracellular ROS levels confirmed that Nrf2 silencing significantly upregulated intracellular ROS levels compared with Si-NC group, further suggesting that CA exerts antioxidant effects through Nrf2 (Fig. 7B). Western blotting results revealed that compared with the Si-NC group, Si-Nrf2 significantly reduced Nrf2 protein expression levels. Compared with the Si-NC group, Nrf2 silencing in the Si-Nrf2 group significantly upregulated the expression levels of TXNIP, activated NLRP3 inflammasome, and increased the expression levels of NLRP3, ASC, pro- and cleaved-caspase-1, GSDMD, GSDMD-NT, IL-18 and IL-1β, further confirming that Nrf2 silencing reversed the inhibitory effect of CA on pyroptosis (Fig. 7C-E).

Discussion

There is a consensus that inflammation, oxidative stress, mitochondrial dysfunction and cell death serve a central role in the progression of HF (7,8,26). However, the specific mechanisms of pyroptosis and effective interventions in HF remain unclear, especially since previous studies have revealed that pyroptosis also mediates mitochondrial damage in cells (13,27). To the best of our knowledge, the present study is the first to systematically investigate the therapeutic mechanism of CA to attenuate mitochondrial damage and pyroptosis in HF via the Nrf2/ROS/TXNIP pathway, which not only demonstrated the cardioprotective effects of CA, but also confirmed the complex interactions between oxidative stress, mitochondrial damage and pyroptosis. Therefore, the present study proposes the Nrf2/ROS/TXNIP pathway as a potentially promising therapeutic target for treating mitochondrial damage and pyroptosis in HF.

The natural flavonoid compound CA is the main bioactive chemical in Radix Astragali, and has been shown to exert anti-HF therapeutic effects (17-20). Previous studies have demonstrated that CA regulates oxidative stress by modulating

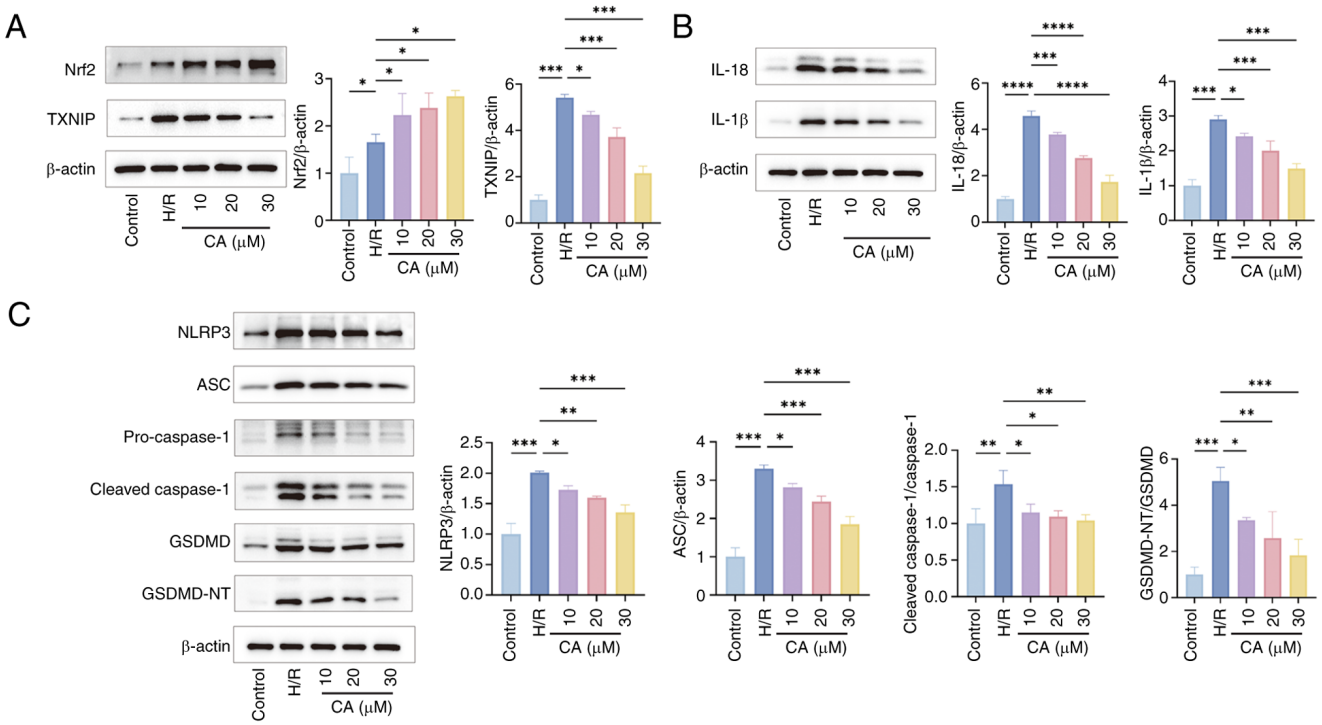

Figure 5. CA inhibits pyroptosis via the Nrf2/reactive oxygen species/TXNIP pathway (n=3). (A) Representative images of the expression levels and semi-quantitative analysis of Nrf2 and TXNIP in cells by western blotting (n=3). (B) and semi-quantitative analysis and semi-quantitative analysis of IL-18 and IL-1β in cells by western blotting and (n=3). (C) and semi-quantitative analysis and semi-quantitative analysis of levels of NLRP3, ASC, pro- and cleaved-caspase-1, GSDMD, GSDMD-NT in cells by western blotting (n=3). Data are presented as the mean ± SD, *P<0.05, **P<0.01, ***P<0.001. CA, calycosin; Nrf2, nuclear factor erythroid 2-related factor; TXNIP, thioredoxin-interacting protein; H/R, hypoxia-reperfusion, ASC, apoptosis-associated speck-like protein containing a CARD; GSDMD, gasdermin D; GSDMD-NT, GSDMD N-terminal fragments; NLRP3, NLR family pyrin domain-containing protein 3.

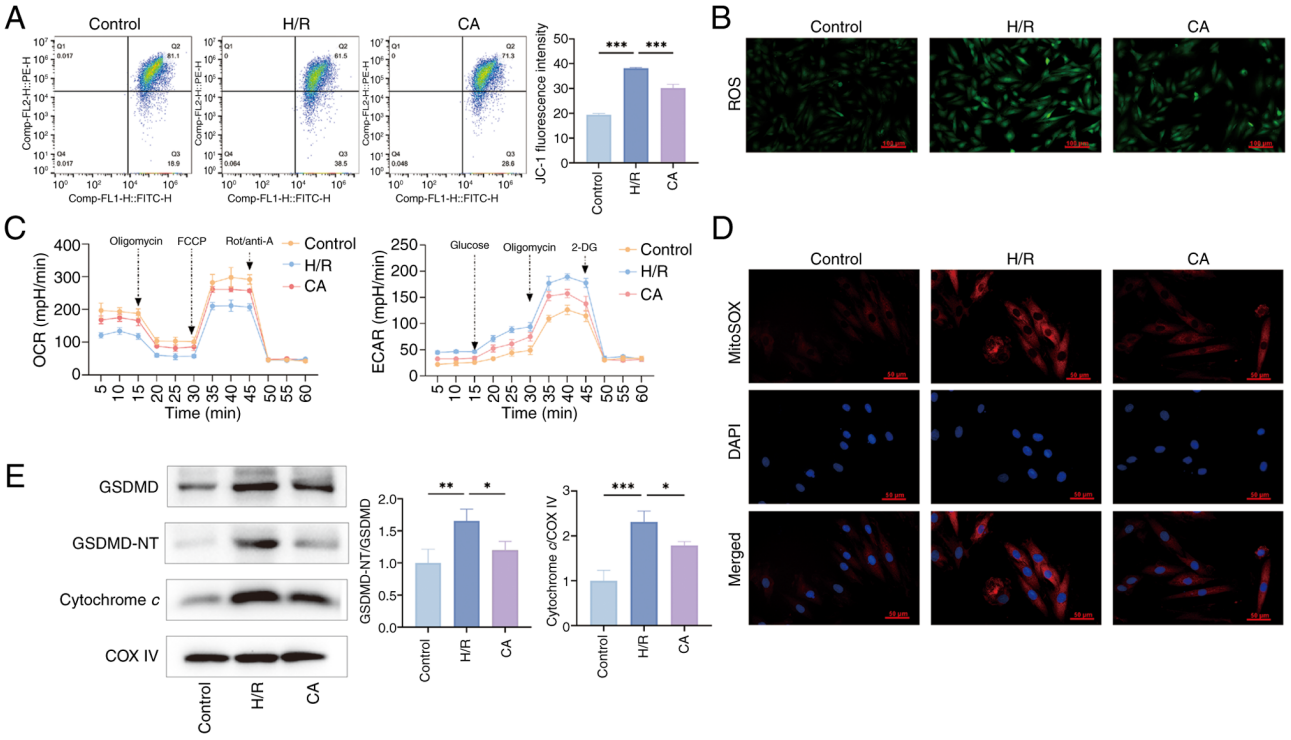

Figure 6. CA improves mitochondrial damage in cardiomyocytes. (A) Flow cytometric analysis of JC-1 staining was used to detect changes in mitochondrial membrane potential (n=3). (B) Representative intracellular ROS staining images of each group. (C) Representative mitochondrial ROS staining images of each group. (D) ECAR and OCR of cardiomyocytes were assessed (n=3). (E) Expression levels of GSDMD, GSDMD-NT and cytochrome *c* proteins were examined by western blotting (n=3). COX IV was used as a loading control in mitochondria. Data are presented as the mean ± SD, *P<0.05, **P<0.01, ***P<0.001. CA, calycosin; ROS, reactive oxygen species; ECAR, extracellular acidification rate; OCR, oxygen consumption rate; FCCP, Trifluoromethoxy carbonylcyanide phenylhydrazone, Carbonyl cyanide 4-(trifluoromethoxy)phenylhydrazone; Rot/anti-A, rotenone/antimycin A; GSDMD, gasdermin D; GSDMD-NT, GSDMD N-terminal fragments; H/R, hypoxia-reperfusion.

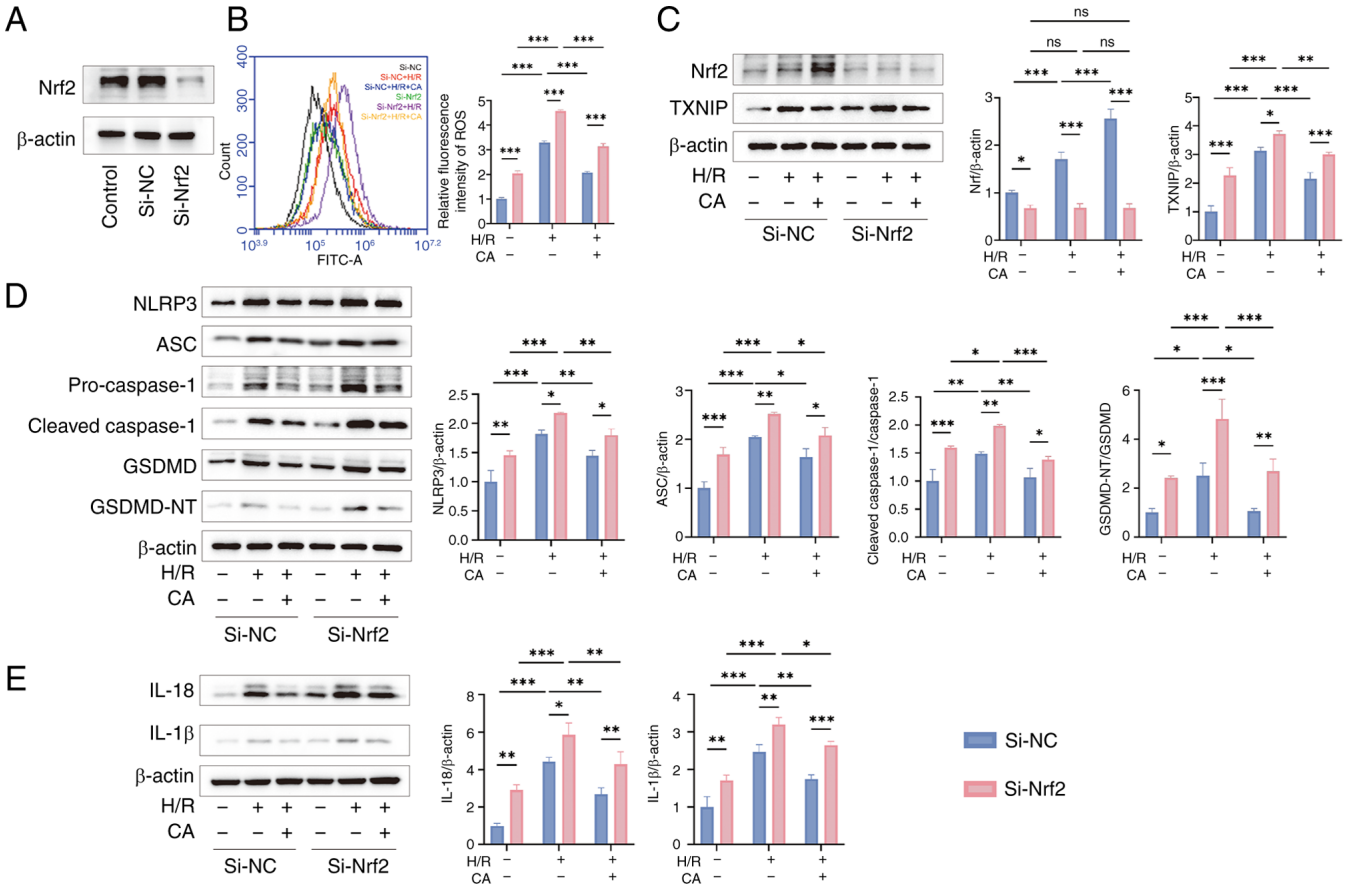

Figure 7. Silencing Nrf2 inhibits the therapeutic effects of CA. (A) Transfection efficiency of si-Nrf2. (B) Detection of intracellular ROS levels in each group (n=3). (C) Representative images and semi-quantitative analysis of Nrf2 and TXNIP in cells by western blotting (n=3). (D) Representative images and semi-quantitative analysis of NLRP3, ASC, pro- and cleaved-caspase-1, GSDMD, GSDMD-NT in cells by western blotting (n=3). (E) Representative images and semi-quantitative analysis levels of IL-18 and IL-1β in cells by western blotting (n=3). Data are presented as the mean ± SD, *P<0.05, **P<0.01, ***P<0.001, ns, no significance. si, small interfering; CA, calycosin; Nrf2, nuclear factor erythroid 2-related factor; ROS, reactive oxygen species; TXNIP, thioredoxin-interacting protein; ASC, apoptosis-associated speck-like protein containing a CARD; NLRP3, NLR family pyrin domain-containing protein 3; GSDMD, gasdermin D; GSDMD-NT, GSDMD N-terminal fragments; H/R, hypoxia-reperfusion; NC, negative control.

Nrf2 expression (28,29), but the specific mechanism remains to be investigated. Previous studies have demonstrated that CA inhibits NLRP3 inflammasome activation-mediated pyroptosis and ameliorates myocardial injury (21,22). However, these studies mainly focused on phenotypes and downstream effector proteins, while the effects on upstream signaling pathways were insufficiently studied, resulting in an incomplete understanding of the mechanism of CA treatment. Meanwhile, another study revealed that CA upregulates Nrf2 expression levels, and alleviates myocardial oxidative stress and mitochondrial damage, thereby protecting the myocardium (21), warranting further investigation of the effect of CA on Nrf2 regulation and pyroptosis in the failing myocardium. The present study indicated that CA improved cardiac function, attenuated cardiac oxidative stress, and prevented myocardial fibrosis and inflammatory injury in HF via the Nrf2/ROS/TXNIP pathway, demonstrating the complex interactions between oxidative stress, mitochondrial damage and pyroptosis.

Nrf2 is a key regulator of cellular defense mechanisms, particularly regulating cellular antioxidant responses under oxidative stress conditions (15). During oxidative stress, Nrf2 dissociates from Kelch-like ECH-associated protein 1 (Keap1), translocates to the nucleus and activates the transcription of antioxidant-responsive genes, enhancing ROS cellular scavenging (30). TXNIP is a negative regulator downstream of Nrf2/ROS. The activation of Nrf2 reduces ROS levels, thereby inhibiting ROS-mediated dissociation of TXNIP and TRX, and consequently attenuating TXNIP expression (31,32). Downregulation of TXNIP weakens the interaction between TXNIP and NLRP3, thereby suppressing NLRP3 inflammasome activation and ultimately attenuating pyroptosis and inflammatory responses (33,34). Therefore, Nrf2 is a key factor linking oxidative stress and NLRP3 inflammasome activation. Considerable oxidative stress is present in HF (8), resulting in elevated Nrf2 levels, but this elevation is limited (35). Therefore, although Nrf2 expression is elevated, it is insufficient to completely counteract the complex inflammatory response and oxidative stress, therefore TXNIP expression remains high in HF (36-38). The present study has found that both Nrf2 and TXNIP expression were upregulated in HF, consistent with previous research findings. In the present study, CA treatment was shown to improve oxidative stress indicators, such as LDH, MDA, SOD and T-GSH/GSSG, in HF-induced rats. Western blotting and flow cytometry results also confirmed that CA treatment upregulated Nrf2 expression, decreased ROS levels, and inhibited the expression of

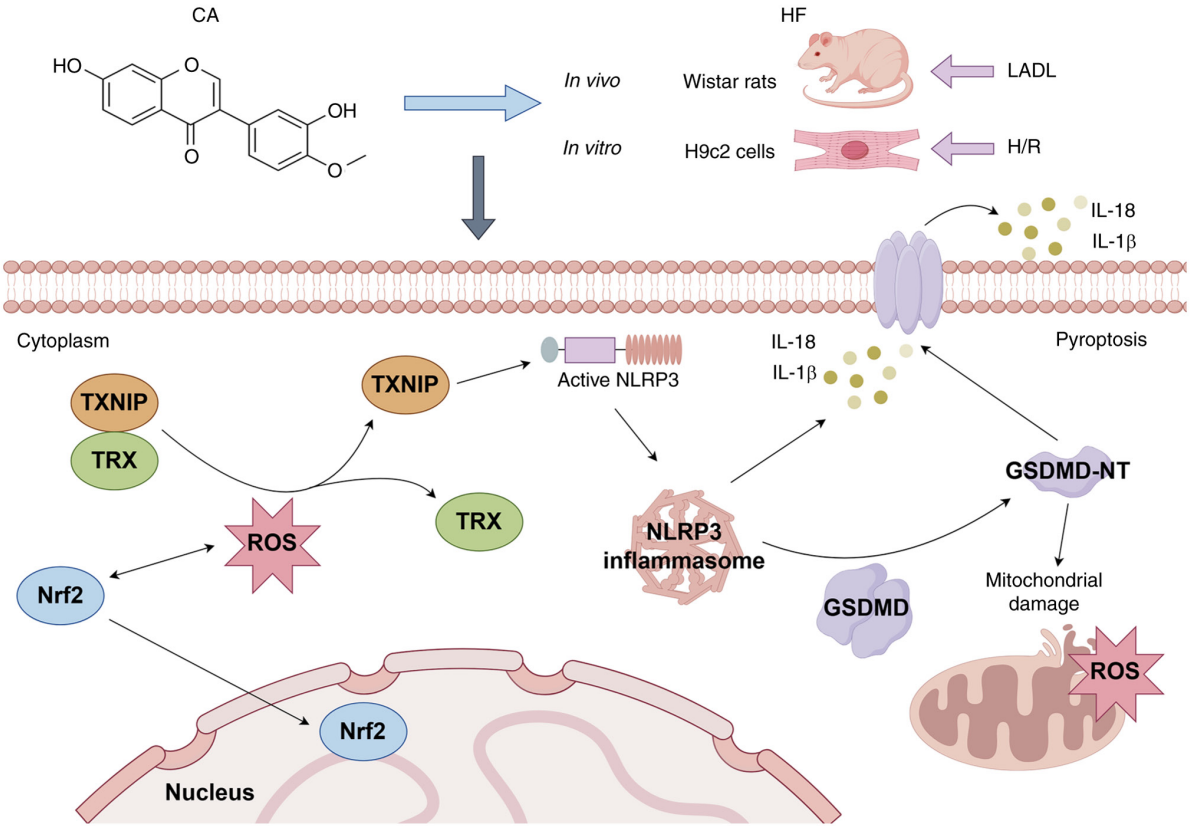

Figure 8. Molecular mechanisms of CA treatment for HF. CA promotes Nrf2 expression and its nuclear translocation, thereby alleviating mitochondrial damage and pyroptosis in HF via the Nrf2/ROS/TXNIP pathway. This figure was generated by FigDraw. CA, calycosin; HF, heart failure; LADL, left anterior descending ligation; Nrf2, nuclear factor erythroid 2-related factor; ROS, reactive oxygen species; TRX, thioredoxin; TXNIP, thioredoxin-interacting protein; H/R, hypoxia-reoxygenation; NLRP3, NLR family pyrin domain-containing protein 3; GSDMD, gasdermin D; GSDMD-NT, GSDMD N-terminal fragments.

TXNIP and corresponding pyroptosis proteins. Nrf2 immunofluorescence experiments revealed that CA treatment elevated Nrf2 expression levels and confirmed its nuclear translocation. These results highlight the role of Nrf2 in the treatment of HF with CA.

To further confirm the central role of Nrf2 in the anti-HF effects of CA, the present study used siRNA to silence Nrf2. The results revealed that compared to the Si-NC group, silencing Nrf2 markedly reduced the protective effects of CA, including a significant increase in ROS levels and the expression of downstream molecules. However, the natural compound CA has multi-pathway, multi-target therapeutic advantages and its therapeutic mechanism may involve the synergistic action of multiple signaling pathways. Studies have revealed that CA can improve myocardial fibrosis and cardiac dysfunction through the TGFBR1 signaling pathway and can also inhibit inflammation and fibrosis in HF-induced rats through the AKT-IKK/STAT3 axis (19,20).

Pyroptosis, a form of programmed cell death mediated by GSDMD, has been reported to serve a key role in the pathological process of HF, exacerbating inflammation and tissue damage (11). Specifically, GSDMD is activated by specific signals and undergoes a conformational change into GSDMD-NT, which perforates the cell membrane, leading to leakage of cellular contents and cellular swelling, ultimately triggering cell rupture and death (12,39). The significant inflammatory response and oxidative stress present in HF can activate multiple pathways, such as the NF-κB signaling pathway that promotes GSDMD and Caspase-1 transcription and synthesis. The *in vivo* and *in vitro* results further confirmed that CA effectively suppressed this synthesis. Furthermore, it inhibited NLRP3 inflammasome activation, thereby suppressing the further cleavage and activation of GSDMD and Caspase-1, suggesting that CA inhibits pyroptosis in failing cardiomyocytes. Mitochondrial dysfunction is involved in a variety of pathological mechanisms such as disturbed energy metabolism, dysregulation of calcium homeostasis, inflammatory response and cell death, and has emerged as a key target for HF (40). A recent study confirmed that activation of GSDMD-NT during pyroptosis leads not only to perforated rupture of cellular membranes, but also to perforation of mitochondrial membranes, which in turn leads to mitochondrial damage and release of ROS (13). Pyroptosis driven by GSDMD not only leads to myocardial damage but also amplifies mitochondrial damage and promotes the process toward HF. The crosstalk between pyroptosis and mitochondrial dysfunction underscores the complexity of HF pathophysiology. In the present study, CA treatment not only attenuated pyroptosis but also ameliorated mitochondrial damage. TEM examination of HF rats revealed that CA improved mitochondrial ultrastructure and *in vitro* cellular experiments further demonstrated that CA treatment downregulated the expression of mitochondrial GSDMD-NT and improved mitochondrial membrane potential, mitochondrial ROS levels and mitochondrial respiration, which suggests that CA exerts its cardioprotective effects through multiple pathways (Fig. 8).

Natural compounds have demonstrated promising potential in the treatment of HF due to their multi-targeting properties, low side effects, and excellent anti-inflammatory and antioxidant effects (41-43). Compared with other similar natural compounds that modulate Nrf2, such as sulforaphane and curcumin, CA has unique advantages and preclinical therapeutic potential. Sulforaphane has antioxidant and anti-inflammatory properties and has been shown to improve cardiac function and prevent worsening of HF by regulating Nrf2 expression levels (44). However, CA has a unique advantage because of its ability to inhibit pyroptosis and regulate the process of cell death in cardiomyocytes (21,22). Curcumin has antioxidant, anti-apoptotic and anti-inflammatory properties, and has been shown to improve HF by ameliorating ventricular hypertrophy and inhibiting myocardial fibrosis (45,46). However, the low stability of curcumin limits its further clinical translation (47). By contrast, CA has improved stability and may be a more suitable choice for the clinical treatment of HF.

The present study used LAD ligation to establish the HF model and demonstrated that CA improved cardiac function and myocardial damage, suppressed myocardial oxidative stress and improved mitochondrial ultrastructure in HF-induced rats. However, the LAD ligation model is widely used to study ischemic HF, as it simulates the pathophysiological characteristics of human ischemic HF by inducing local myocardial ischemia (48), which may not reflect the pathological changes and cardiac remodeling specific to non-ischemic HF. In H9c2 cells, the present study used the H/R model to simulate HF and further confirmed the therapeutic mechanism of CA against HF. However, the H/R model simulates myocardial ischemia-reperfusion injury, which captures the key initiating mechanisms associated with ischemia-reperfusion stress injury, but cannot fully reflect the complex, chronic adaptive and maladaptive processes of chronic HF, whether of ischemic or non-ischemic origin (49).

Notably, several limitations should be acknowledged. Firstly, the LAD ligation model primarily simulates ischemic HF, and the H/R model in H9c2 cells, although capable of capturing the key mechanisms of myocardial ischemia-reperfusion stress injury, may not fully reflect the pathophysiology of chronic HF. The detection of ROS data at a single time point limits dynamic understanding of oxidative stress in HF, therefore, this should be further investigated using multiple time points. Furthermore, H9c2 cells are widely used in studies related to cardiovascular disease (50-52), but they cannot fully represent the physiological characteristics of primary cardiomyocytes. Future studies should use primary cells to provide an improved simulation of the pathophysiological progression of HF. Secondly, the present study showed that CA inhibits pyroptosis in HF and improves mitochondrial damage, possibly disrupting the crosstalk between mitochondrial damage and pyroptosis. However, the exact mechanism remains to be further validated through experiments such as co-immunoprecipitation or proximity ligation assays to determine the interaction between GSDMD-NT and mitochondria or using cytosolic fractions to confirm mitochondrial outer membrane permeabilization. Nrf2 silencing eliminated the protective effect of CA; however, it remains unclear as to whether the effects of CA are directly mediated by Nrf2 or through upstream/downstream interactions. Therefore, additional validation is needed, including experiments such as Nrf2 overexpression rescue after Nrf2 knockdown, or TXNIP knockout and Keap1-Nrf2 interaction after Nrf2 knockdown to confirm the specificity of Nrf2 and causality. Finally, the present study is a preclinical basic study, which is a preliminary exploration of the pharmacological efficacy of CA. The clinical translational application of CA requires further evaluation of aspects such as pharmacokinetics (bioavailability, tissue distribution and metabolic stability) and safety. The sample size of some experiments in the present study was also relatively small; although consistent trends were observed in repeated measurements, a larger sample size would enhance the accuracy and scientific validity of the present study.

To the best of our knowledge, the present study demonstrated, for the first time, that CA possibly disrupts the crosstalk between pyroptosis-mitochondrial damage in HF via the Nrf2/ROS/TXNIP pathway. CA may attenuate the activation of upstream triggers of pyroptosis, ROS overproduction and downregulate the downstream actuator protein, GSDMD-NT, thereby ameliorating cardiac function and myocardial injury in HF. However, additional validation is still required to further confirm the specificity of Nrf2 in CA treatment.

Acknowledgements

Not applicable.

Funding

This work was supported by the Natural Science Foundation of Shandong Province (grant no. ZR2023MH053).

Availability of data and materials

The data generated in the present study may be requested from the corresponding author.

Authors' contributions

HJY, YDY, YTX and YL conceived the study. HJY, QCH and HY carried out the experiments. YDY and XJL analyzed the data. HJY and QCH drafted the manuscript. YTX and YL reviewed and revised the manuscript. YTX and YL confirm the authenticity of all the raw data. All authors read and approved the final manuscript.

Ethics approval and consent to participate

The animal experiment was reviewed and approved by the Experimental Animal Management Committee and the Ethics Committee of the Affiliated Hospital of Shandong University of Traditional Chinese Medicine (approval no. SDSZYYAWE20231031001).

Patient consent for publication

Not applicable.

Competing interests

The authors declare that they have no competing interests.

References

1. Tsao CW, Aday AW, Almarzooq ZI, Anderson CAM, Arora P, Avery CL, Baker-Smith CM, Beaton AZ, Boehme AK, Buxton AE, *et al*: Heart disease and stroke statistics-2023 update: A report from the American heart association. Circulation 147: e93-e621, 2023.
2. Khan MS, Shahid I, Bennis A, Rakisheva A, Metra M and Butler J: Global epidemiology of heart failure. Nat Rev Cardiol 21: 717-734, 2024.
3. Bozkurt B, Fonarow GC, Goldberg LR, Guglin M, Josephson RA, Forman DE, Lin G, Lindenfeld J, O'Connor C, Panjrath G, *et al*: Cardiac rehabilitation for patients with heart failure: JACC expert panel. J Am Coll Cardiol 77: 1454-1469, 2021.
4. Zannad F, O'Connor CM, Butler J, McMullan CJ, Anstrom KJ, Barash I, Bonaca MP, Borentain M, Corda S, Gates D, *et al*: Vericiguat for patients with heart failure and reduced ejection fraction across the risk spectrum: An individual participant data analysis of the VICTORIA and VICTOR trials. Lancet: August 30, 2025 (Epub ahead of print).
5. Cools JMT, Goovaerts BK, Feyen E, Van den Bogaert S, Fu Y, Civati C, Van Fraeyenhove J, Tubeeckx MRL, Ott J, Nguyen L, *et al*: Small-molecule-induced ERBB4 activation to treat heart failure. Nat Commun 16: 576, 2025.
6. Rossignol P, Hernandez AF, Solomon SD and Zannad F: Heart failure drug treatment. Lancet 393: 1034-1044, 2019.
7. Brown DA, Perry JB, Allen ME, Sabbah HN, Stauffer BL, Shaikh SR, Cleland JG, Colucci WS, Butler J, Voors AA, *et al*: Expert consensus document: Mitochondrial function as a therapeutic target in heart failure. Nat Rev Cardiol 14: 238-250, 2017.
8. van der Pol A, van Gilst WH, Voors AA and van der Meer P: Treating oxidative stress in heart failure: Past, present and future. Eur J Heart Fail 21: 425-435, 2019.
9. Dridi H, Kushnir A, Zalk R, Yuan Q, Melville Z and Marks AR: Intracellular calcium leak in heart failure and atrial fibrillation: A unifying mechanism and therapeutic target. Nat Rev Cardiol 17: 732-747, 2020.
10. Xiang Q, Yi X, Zhu XH, Wei X and Jiang DS: Regulated cell death in myocardial ischemia-reperfusion injury. Trends Endocrinol Metab 35: 219-234, 2024.
11. Zhang Z, Yang Z, Wang S, Wang X and Mao J: Overview of pyroptosis mechanism and in-depth analysis of cardiomyocyte pyroptosis mediated by NF-κB pathway in heart failure. Biomed Pharmacother 179: 117367, 2024.
12. Shi J, Zhao Y, Wang K, Shi X, Wang Y, Huang H, Zhuang Y, Cai T, Wang F and Shao F: Cleavage of GSDMD by inflammatory caspases determines pyroptotic cell death. Nature 526: 660-665, 2015.
13. Miao R, Jiang C, Chang WY, Zhang H, An J, Ho F, Chen P, Zhang H, Junqueira C, Amgalan D, *et al*: Gasdermin D permeabilization of mitochondrial inner and outer membranes accelerates and enhances pyroptosis. Immunity 56: 2523-2541.e8, 2023.
14. Zhou R, Tardivel A, Thorens B, Choi I and Tschopp J: Thioredoxin-interacting protein links oxidative stress to inflammasome activation. Nat Immunol 11: 136-140, 2010.
15. Morgenstern C, Lastres-Becker I, Demirdöğen BC, Costa VM, Daiber A, Foresti R, Motterlini R, Kalyoncu S, Arioz BI, Genc S, *et al*: Biomarkers of NRF2 signalling: Current status and future challenges. Redox Biol 72: 103134, 2024.
16. Sies H and Jones DP: Reactive oxygen species (ROS) as pleiotropic physiological signalling agents. Nat Rev Mol Cell Biol 21: 363-383, 2020.
17. Deng M, Chen H, Long J, Song J, Xie L and Li X: Calycosin: A review of its pharmacological effects and application prospects. Expert Rev Anti Infect Ther 19: 911-925, 2021.
18. Ding WJ, Chen GH, Deng SH, Zeng KF, Lin KL, Deng B, Zhang SW, Tan ZB, Xu YC, Chen S, *et al*: Calycosin protects against oxidative stress-induced cardiomyocyte apoptosis by activating aldehyde dehydrogenase 2. Phytother Res 37: 35-49, 2023.
19. Wang X, Li W, Zhang Y, Sun Q, Cao J, Tan N, Yang S, Lu L, Zhang Q, Wei P, *et al*: Calycosin as a Novel PI3K activator reduces inflammation and fibrosis in heart failure through AKT-IKK/STAT3 axis. Front Pharmacol 13: 828061, 2022.
20. Chen G, Xu H, Xu T, Ding W, Zhang G, Hua Y, Wu Y, Han X, Xie L, Liu B and Zhou Y: Calycosin reduces myocardial fibrosis and improves cardiac function in post-myocardial infarction mice by suppressing TGFBR1 signaling pathways. Phytomedicine 104: 154277, 2022.
21. Zhang L, Fan C, Jiao HC, Zhang Q, Jiang YH, Cui J, Liu Y, Jiang YH, Zhang J, Yang MQ, *et al*: Calycosin alleviates doxorubicin-induced cardiotoxicity and pyroptosis by inhibiting NLRP3 inflammasome activation. Oxid Med Cell Longev 2022: 1733834, 2022.
22. Yuan HJ, Han QC, Yu H, Yu YD, Liu XJ, Xue YT and Li Y: Calycosin treats acute myocardial infarction via NLRP3 inflammasome: Bioinformatics, network pharmacology and experimental validation. Eur J Pharmacol 997: 177621, 2025.
23. Han Q, Shi J, Yu Y, Yuan H, Guo Y, Liu X, Xue Y and Li Y: Calycosin alleviates ferroptosis and attenuates doxorubicin-induced myocardial injury via the Nrf2/SLC7A11/GPX4 signaling pathway. Front Pharmacol 15: 1497733, 2024.
24. Xu S, Huang P, Yang J, Du H, Wan H and He Y: Calycosin alleviates cerebral ischemia/reperfusion injury by repressing autophagy via STAT3/FOXO3a signaling pathway. Phytomedicine 115: 154845, 2023.
25. Jiang Q, Chen X, Gong K, Xu Z, Chen L and Zhang F: M6a demethylase FTO regulates the oxidative stress, mitochondrial biogenesis of cardiomyocytes and PGC-1a stability in myocardial ischemia-reperfusion injury. Redox Rep 30: 2454892, 2025.
26. Del Re DP, Amgalan D, Linkermann A, Liu Q and Kitsis RN: Fundamental mechanisms of regulated cell death and implications for heart disease. Physiol Rev 99: 1765-1817, 2019.
27. Evavold CL, Hafner-Bratkovič I, Devant P, D'Andrea JM, Ngwa EM, Boršić E, Doench JG, LaFleur MW, Sharpe AH, Thiagarajah JR and Kagan JC: Control of gasdermin D oligomerization and pyroptosis by the ragulator-Rag-mTORC1 pathway. Cell 184: 4495-4511.e19, 2021.
28. Qi XM, Zhang WZ, Zuo YQ, Qiao YB, Zhang YL, Ren JH and Li QS: Nrf2/NRF1 signaling activation and crosstalk amplify mitochondrial biogenesis in the treatment of triptolide-induced cardiotoxicity using calycosin. Cell Biol Toxicol 41: 2, 2024.
29. Lu CY, Day CH, Kuo CH, Wang TF, Ho TJ, Lai PF, Chen RJ, Yao CH, Viswanadha VP, Kuo WW and Huang CY: Calycosin alleviates H_2O_2-induced astrocyte injury by restricting oxidative stress through the Akt/Nrf2/HO-1 signaling pathway. Environ Toxicol 37: 858-867, 2022.
30. Kobayashi EH, Suzuki T, Funayama R, Nagashima T, Hayashi M, Sekine H, Tanaka N, Moriguchi T, Motohashi H, Nakayama K and Yamamoto M: Nrf2 suppresses macrophage inflammatory response by blocking proinflammatory cytokine transcription. Nat Commun 7: 11624, 2016.
31. Zhang J, Li X, Han X, Liu R and Fang J: Targeting the thioredoxin system for cancer therapy. Trends Pharmacol Sci 38: 794-808, 2017.
32. Chen Y, Cao X, Pan B, Du H, Li B, Yang X, Chen X, Wang X, Zhou T, Qin A, *et al*: Verapamil attenuates intervertebral disc degeneration by suppressing ROS overproduction and pyroptosis via targeting the Nrf2/TXNIP/NLRP3 axis in four-week puncture-induced rat models both in vivo and in vitro. Int Immunopharmacol 123: 110789, 2023.
33. Choi EH and Park SJ: TXNIP: A key protein in the cellular stress response pathway and a potential therapeutic target. Exp Mol Med 55: 1348-1356, 2023.
34. Abderrazak A, Syrovets T, Couchie D, El Hadri K, Friguet B, Simmet T and Rouis M: NLRP3 inflammasome: From a danger signal sensor to a regulatory node of oxidative stress and inflammatory diseases. Redox Biol 4: 296-307, 2015.
35. Lu Y, An L, Taylor MRG and Chen QM: Nrf2 signaling in heart failure: Expression of Nrf2, Keap1, antioxidant, and detoxification genes in dilated or ischemic cardiomyopathy. Physiol Genomics 54: 115-127, 2022.
36. Wang B, Jin Y, Liu J, Liu Q, Shen Y, Zuo S and Yu Y: EP1 activation inhibits doxorubicin-cardiomyocyte ferroptosis via Nrf2. Redox Biol 65: 102825, 2023.
37. Zhou P, Yang L, Li R, Yin Y, Xie G, Liu X, Shi L, Tao K and Zhang P: IRG1/itaconate alleviates acute liver injury in septic mice by suppressing NLRP3 expression and its mediated macrophage pyroptosis via regulation of the Nrf2 pathway. Int Immunopharmacol 135: 112277, 2024.
38. Zhan Y, Xu D, Tian Y, Qu X, Sheng M, Lin Y, Ke M, Jiang L, Xia Q, Kaldas FM, *et al*: Novel role of macrophage TXNIP-mediated CYLD-NRF2-OASL1 axis in stress-induced liver inflammation and cell death. JHEP Rep 4: 100532, 2022.
39. Devant P and Kagan JC: Molecular mechanisms of gasdermin D pore-forming activity. Nat Immunol 24: 1064-1075, 2023.
40. Wu C, Zhang Z, Zhang W and Liu X: Mitochondrial dysfunction and mitochondrial therapies in heart failure. Pharmacol Res 175: 106038, 2022.

41. Sunagawa Y, Iwashimizu S, Ono M, Mochizuki S, Iwashita K, Sato R, Shimizu S, Funamoto M, Shimizu K, Hamabe-Horiike T, *et al*: The citrus flavonoid nobiletin prevents the development of doxorubicin-induced heart failure by inhibiting apoptosis. J Pharmacol Sci 158: 84-94, 2025.
42. Wu Y, Huang X, He Y, Chang J, Fang X, Kang P, Feng N, Liu R, Xiao P, Shi D, *et al*: Mechanism of puerarin alleviating myocardial remodeling through NSUN2-mediated m5C methylation modification. Phytomedicine 143: 156849, 2025.
43. Sun SN, Liu X, Chen XL, Liang SL, Li J, Liao HL, Fang HC, Ni SH, Li Y, Lu L, *et al*: Calycosin alleviates myocardial fibrosis after myocardial infarction by restoring fatty acid metabolism homeostasis through inhibiting FAP. Phytomedicine 145: 157045, 2025.
44. Bai Y, Chen Q, Sun YP, Wang X, Lv L, Zhang LP, Liu JS, Zhao S and Wang XL: Sulforaphane protection against the development of doxorubicin-induced chronic heart failure is associated with Nrf2 upregulation. Cardiovasc Ther 35, 2017.
45. Jiang S, Han J, Li T, Xin Z, Ma Z, Di W, Hu W, Gong B, Di S, Wang D and Yang Y: Curcumin as a potential protective compound against cardiac diseases. Pharmacol Res 119: 373-383, 2017.
46. Saeidinia A, Keihanian F, Butler AE, Bagheri RK, Atkin SL and Sahebkar A: Curcumin in heart failure: A choice for complementary therapy? Pharmacol Res 131: 112-119, 2018.
47. Pan Y, Zhu G, Wang Y, Cai L, Cai Y, Hu J, Li Y, Yan Y, Wang Z, Li X, *et al*: Attenuation of high-glucose-induced inflammatory response by a novel curcumin derivative B06 contributes to its protection from diabetic pathogenic changes in rat kidney and heart. J Nutr Biochem 24: 146-155, 2013.
48. Grilo GA, Munoz J Jr, Lee DH, Hossain S, Ma Y, Kain V, Lindsey ML and Halade GV: Macro- and microinjury define the heart failure progression after permanent coronary ligation or ischemia-reperfusion in young healthy mice. Am J Physiol Heart Circ Physiol 329: H521-H533, 2025.
49. Heusch G: Molecular basis of cardioprotection: Signal transduction in ischemic pre-, post-, and remote conditioning. Circ Res 116: 674-699, 2015.
50. Laudette M, Lindbom M, Cinato M, Bergh PO, Skålén K, Arif M, Miljanovic A, Czuba T, Perkins R, Smith JG, *et al*: PCSK9 regulates cardiac mitochondrial cholesterol by promoting TSPO degradation. Circ Res 136: 924-942, 2025.
51. Khodade VS, Liu Q, Zhang C, Keceli G, Paolocci N and Toscano JP: Arylsulfonothioates: Thiol-activated donors of hydropersulfides which are excreted to maintain cellular redox homeostasis or retained to counter oxidative stress. J Am Chem Soc 147: 7765-7776, 2025.
52. Zhao ST, Qiu ZC, Xu ZQ, Tao ED, Qiu RB, Peng HZ, Zhou LF, Zeng RY, Lai SQ and Wan L: Curcumin attenuates myocardial ischemia-reperfusion-induced autophagy-dependent ferroptosis via Sirt1/AKT/FoxO3a signaling. Int J Mol Med 55: 51, 2025.